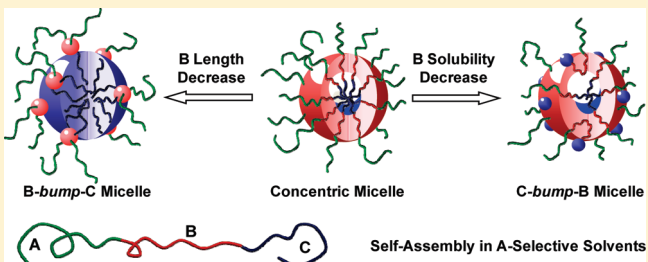


## Structural Evolution of Multicompartment Micelles Self-Assembled from Linear ABC Triblock Copolymer in Selective Solvents

Tao Jiang, Liquan Wang, Shaoliang Lin, Jiaping Lin,\* and Yongliang Li

Shanghai Key Laboratory of Advanced Polymeric Materials, Key Laboratory for Ultrafine Materials of Ministry of Education, State Key Laboratory of Bioreactor Engineering, School of Materials Science and Engineering, East China University of Science and Technology, Shanghai 200237, China

**ABSTRACT:** Using dissipative particle dynamics simulation, structural evolution from concentric multicompartment micelles to raspberry-like multicompartment micelles self-assembled from linear ABC triblock copolymers in selective solvents was investigated. The structural transformation from concentric micelles to raspberry-like micelles can be controlled by changing either the length of B blocks or the solubility of B block. It was found that the structures with B bumps on C surface (*B-bump-C*) are formed at shorter B block length and the structures with C bumps on B surface (*C-bump-B*) are formed at relative lower solubility of B blocks. The formation of *B-bump-C* is entropy-driven, while the formation of *C-bump-B* is enthalpy-dominated. Furthermore, when the length of C blocks is much lower than that of B blocks, an inner-penetrating vesicle was discovered. The results gained through the simulations provide an insight into the mechanism behind the formation of raspberry-like micelles.



### 1. INTRODUCTION

Amphiphilic block copolymers, consisting of solvophilic and solvophobic blocks, can self-assemble into kinds of ordered nanoscale structures, such as spherical micelles, cylindrical micelles, and vesicles in selective solvents.<sup>1–7</sup> To date, the self-assembly mechanism of amphiphilic diblock copolymers in dilute solution is well-documented.<sup>8–11</sup> In contrast with the diblock copolymers, the self-assembly of ABC triblock copolymers in selective solvents is more complicated<sup>12,13</sup> and thereby needs to be explored further. The ABC triblock copolymers are capable of forming a variety of complex micelles called multicompartment micelles, which are composed of a solvophilic shell and a segregated solvophobic core. The multicompartment micelles have received considerable attention due to the potential applications in biomedicine and nanotechnology.<sup>14,15</sup>

Multicompartment micelles, e.g., segmented-worm micelles, have been frequently found in the solution system of ABC miktoarm star copolymers.<sup>16,17</sup> The miktoarm star copolymers have been found to be particularly suited for preparing the multicompartment micelles. In addition to the well-studied miktoarm star copolymers, linear triblock copolymers are also able to self-assemble into multicompartment micelles. When two of the blocks are soluble in the solvents, the linear ABC triblock copolymer can only form micelles with a solvophobic inner core and a shell composed of two solvophilic blocks.<sup>18,19</sup> However, when two of the blocks are insoluble in the solvents, for example, a “solvophilic–solvophobic–solvophobic” architecture, the self-assembly of linear ABC triblock copolymers becomes more complicated and can result in a diversity of multicompartment

micelles including core–shell–corona micelles and raspberry-like micelles, etc. The core–shell–corona structure belongs to structure-in-structure (e.g., spheres in spheres), while the raspberry-like structure proposed by Stadler et al. belongs to structure-on-structure (e.g., spheres on spheres).<sup>20</sup> So far, many examples of core–shell–corona structure, i.e., three-layered concentric micelles, formed by the linear triblock copolymers are reported in the literature.<sup>21–29</sup> For example, Gohy et al. found a core–shell–corona micelle formed by a triblock copolymer of polystyrene-*b*-poly(2-vinylpyridine)-*b*-poly(ethylene oxide) (PS-*b*-P2VP-*b*-PEO) in the aqueous solution.<sup>24</sup> The core–shell–corona micelle consists of a PS core, an intermediate P2VP layer, and a PEO corona. However, studies on the raspberry-like micelles from the linear ABC triblock copolymers are limited.<sup>30–40</sup> Recently, Laschewsky and co-workers reported a raspberry-like micelle self-assembled from a triblock copolymer of poly(4-methyl-4-(4-vinylbenzyl)morpholin-4-ium chloride)-*b*-polystyrene-*b*-poly(pentafluorophenyl 4-vinylbenzyl ether) (PVBM-*b*-PS-*b*-PVBFP) in aqueous medium.<sup>30</sup> The raspberry-like micelles are sphere-on-sphere structures, where the small spheres are formed by the fluorocarbon moieties of PVBFP and the large spherical matrix is the hydrocarbon domains of both PS and PVBFP. Similarly, Ma et al. demonstrated that the polystyrene-*b*-polybutadiene-*b*-poly(2-vinylpyridine) (PS-*b*-PB-*b*-P2VP) triblock copolymers can form spherical micelles with bumped

**Received:** March 22, 2011

**Revised:** April 9, 2011

**Published:** April 20, 2011

surfaces in selective solvent mixtures of toluene and methanol.<sup>38</sup> The above experiments reveal that the “solvophilic–solvophobic–solvophobic” linear ABC triblock copolymers are capable of forming not only concentric structure-in-structure micelles but also bumped structure-on-structure micelles.

From the experimental results obtained so far, it was recognized that there is a large parameter space, e.g., molecule architecture, block length, and monomer solubility, to control the self-assembly behavior of the block copolymers in solutions. Investigating the influence of various parameters on the morphologies of complex micelles may take a huge amount of experimental efforts. In addition, the experimental difficulties in characterization could limit the fine assessment of the complicated structures. In comparison with the experiments, computer simulations and theoretical methods have emerged as powerful tools for studying complex morphologies, providing more microscopic level information than experiments.<sup>41–43</sup> So far, great efforts have been made to investigate the complex micelles in triblock copolymer solutions through various approaches, such as Monte Carlo simulation,<sup>44</sup> simulated annealing method,<sup>13,45</sup> and self-consistent field theory.<sup>46,47</sup> For the critical demand of larger scale simulation on polymeric behaviors, the dissipative particle dynamics (DPD) method presents more predominant in the mesoscopic simulations. Compared to the atomistic simulations, it can treat a wider range of length and time scales by many orders of magnitude. It has also been effectively employed to understand the self-assembly behavior of linear triblock copolymer in dilute solution.<sup>48–52</sup> For example, Chou et al. used the DPD simulations to investigate the core–shell–corona micelles from linear triblock copolymers.<sup>48</sup> Some interesting morphologies such as incomplete skin-layered micelle and bicore micelle from linear copolymers with different arrangements of blocks were also predicted. Recent experiments demonstrated the linear ABC triblock copolymers are able to form a distinct multicompartment micelle, namely, micelles with bumped structures, beyond the familiar concentric micelles.<sup>21–40</sup> So far, most reports are only concerned about the structure of the multicompartment micelles, but less attention was paid to the underlying principle governing the formation of bumped micelles. Understanding the underlying principle could be of great importance to provide guidelines for preparing novel micelles and facilitate the further nanotechnology applications. Computer simulations would provide a useful tool to study the principle controlling the structure formations in linear ABC triblock copolymer solutions.

In the present work, we performed a dissipative particle dynamics simulation to study the concentric to raspberry-like morphological evolution of multicompartment micelles formed by the amphiphilic ABC triblock copolymers in selective solvents. The effects of the block length and block solubility were examined. The block density distributions within some representative micelles were also studied. The evolution condition and mechanism from concentric micelles to raspberry-like micelles were revealed. In addition, the inner structure differences between the two micelles were illustrated.

## 2. SIMULATION METHOD

**2.1. DPD Method.** Dissipative particle dynamics (DPD) is a particle-based, mesoscopic simulation technique particularly suitable for complex fluids, originally proposed by Hoogerbrugge and Koelman.<sup>53,54</sup> It is a combination of molecular dynamics,

lattice-gas automata, and Langevin dynamics. It obeys Galilean invariance, isotropy, mass conservation, and momentum conservation. In the DPD simulation, a particle having mass  $m$  represents a block or cluster of atoms or molecules moving together in a coherent fashion. These DPD particles are subject to soft potentials and governed by predefined collision rules.<sup>55</sup> The time evolution of the particle system can be found by solving Newton's equations of motion

$$\frac{d\mathbf{r}_i}{dt} = \mathbf{v}_i, \quad m_i \frac{d\mathbf{v}_i}{dt} = \mathbf{f}_i \quad (1)$$

where  $m_i$ ,  $\mathbf{r}_i$ ,  $\mathbf{v}_i$ , and  $\mathbf{f}_i$  denote the mass, position, velocity of the  $i$ th particle, and the acting force on it, respectively. For simplicity, the masses and diameters of the particles are scaled relative to 1.

The time integration of motion equations is done by a modified velocity-Verlet algorithm<sup>56,57</sup>

$$\begin{aligned} \mathbf{r}_i(t + \Delta t) &= \mathbf{r}_i(t) + \Delta t \mathbf{v}_i(t) + \frac{1}{2}(\Delta t)^2 \mathbf{f}_i(t) \\ \tilde{\mathbf{v}}_i(t + \Delta t) &= \mathbf{v}_i(t) + \lambda \Delta t \mathbf{f}_i(t) \\ \mathbf{f}_i(t + \Delta t) &= \mathbf{f}_i(\mathbf{r}(t + \Delta t), \tilde{\mathbf{v}}(t + \Delta t)) \\ \mathbf{v}_i(t + \Delta t) &= \mathbf{v}_i(t) + \frac{1}{2}\Delta t(\mathbf{f}_i(t) + \mathbf{f}_i(t + \Delta t)) \end{aligned} \quad (2)$$

where  $\tilde{\mathbf{v}}_i(t + \Delta t)$  and  $\mathbf{v}_i(t + \Delta t)$  denote the erroneous and modified velocities at  $t + \Delta t$ . We choose  $\lambda = 0.65$  here according to Groot and Warren<sup>56</sup> and time step  $\Delta t = 0.04\tau$  ( $\tau$  is the time unit).

In the method, the force acting on a particle,  $\mathbf{f}_i$ , is a pairwise additive force, consisting of the conservative force ( $\mathbf{F}_{ij}^C$ ), dissipative force ( $\mathbf{F}_{ij}^D$ ), and random force ( $\mathbf{F}_{ij}^R$ )<sup>56</sup>

$$\mathbf{f}_i = \sum_{j \neq i} (\mathbf{F}_{ij}^C + \mathbf{F}_{ij}^D + \mathbf{F}_{ij}^R) \quad (3)$$

The conservative force is a soft repulsion taking the form as follows:<sup>56</sup>

$$\mathbf{F}_{ij}^C = a_{ij} \sqrt{\omega(r_{ij})} \hat{\mathbf{r}}_{ij} \quad (4)$$

where  $a_{ij}$  is the maximum repulsive interaction between particles  $i$  and  $j$ ,  $\mathbf{r}_{ij} = \mathbf{r}_i - \mathbf{r}_j$ ,  $r_{ij} = |\mathbf{r}_{ij}|$ ,  $\hat{\mathbf{r}}_{ij} = \mathbf{r}_{ij}/r_{ij}$ , and  $\omega(r_{ij})$  is the weight function, given by

$$\omega(r_{ij}) = \begin{cases} (1 - r_{ij}/r_c)^2 & (r_{ij} < r_c) \\ 0 & (r_{ij} \geq r_c) \end{cases} \quad (5)$$

according to the study by Groot and Warren,<sup>56</sup> and  $r_c$  is the cutoff radius ( $r_c = 1.0$ ). The dissipative force is a friction force that acts on the relative velocities of particles, defined by<sup>56</sup>

$$\mathbf{F}_{ij}^D = -\gamma \omega^D(r_{ij}) (\hat{\mathbf{r}}_{ij} \cdot \mathbf{v}_{ij}) \hat{\mathbf{r}}_{ij} \quad (6)$$

and the random force, compensating the loss of kinetic energy due to the dissipative force, is defined by<sup>56</sup>

$$\mathbf{F}_{ij}^R = \sigma \omega^R(r_{ij}) \theta_{ij} \hat{\mathbf{r}}_{ij} \quad (7)$$

where  $\mathbf{v}_{ij} = \mathbf{v}_i - \mathbf{v}_j$ ,  $\gamma$  is the friction coefficient,  $\sigma$  is the noise amplitude,  $\omega^D(r_{ij})$  and  $\omega^R(r_{ij})$  are weight functions vanishing for  $r > r_c$  that describe the range of the dissipative and random forces, and  $\theta_{ij}$  is a randomly fluctuating variable with Gaussian statistics:

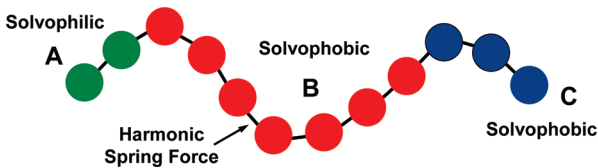


Figure 1. DPD model of an amphiphilic linear ABC triblock copolymer.

$$\begin{aligned}\langle \theta_{ij}(t) \rangle &= 0, \quad \langle \theta_{ij}(t) \theta_{kl}(t') \rangle \\ &= (\delta_{ik} \delta_{jl} + \delta_{il} \delta_{jk}) \delta(t - t')\end{aligned}\quad (8)$$

In order to satisfy the fluctuation–dissipation theorem<sup>56</sup> and for the system to evolve to an equilibrium state that corresponds to the Gibbs canonical ensemble, only one of  $\omega^D(r_{ij})$  and  $\omega^R(r_{ij})$  can be chosen arbitrarily, and the other one is then fixed by the relation<sup>56,58</sup>

$$\omega^D(r_{ij}) = [\omega^R(r_{ij})]^2 = \omega(r_{ij}) \quad (9)$$

And the values of parameters  $\gamma$  and  $\sigma$  are coupled by

$$\sigma^2 = 2\gamma k_B T \quad (10)$$

where  $T$  is the absolute temperature and  $k_B$  is the Boltzmann constant.

In addition, for bonded particles of the linear ABC triblock copolymers, the interaction force is considered as harmonic spring force

$$\mathbf{F}_{ij}^S = C(1 - r_{ij}/r_{eq})\hat{\mathbf{r}}_{ij} \quad (11)$$

In this work, we chose the spring constant  $C = 100$  and the equilibrium bond distance  $r_{eq} = 0.9$ . This choice is only a coarse-graining selection to show the constraint imposed upon connected particles of a polymeric chain. It does not mean that it corresponds to a certain realistic block copolymer. Also, this choice of  $C$  and  $r_{eq}$  does not affect the qualitative behavior of the system.

In the DPD method, reduced units are adopted for all physical quantities.<sup>56</sup> The units of mass, length, time, and energy are defined by  $m$ ,  $r_c$ ,  $\tau$ , and  $k_B T$ , respectively. The time unit  $\tau$  can be obtained by  $\tau = (m r_c^2 / k_B T)^{1/2}$ , and its real value can be estimated by matching the simulated lateral diffusion coefficient to the experimental measured value.

**2.2. Model and Condition.** In the simulations, we constructed a coarse-grained model of amphiphilic linear ABC triblock copolymer with solvophilic A particles and different solvophobic particles (denoted by B and C), as typically shown in Figure 1. The volume fraction of component is variable. The block densities (denoted by  $\varphi_B$ ,  $\varphi_C$ ) are defined as the average particle numbers of unit volume. Additionally, solvent particles (denoted by S) are also included explicitly in the simulation, but the S particles are not shown in figures for clarity.

All the simulations were performed in a simulation box of  $L \times L \times L$ . Periodic boundary conditions and NVT ensemble were adopted. We mainly focused on the  $30 \times 30 \times 30$  DPD units system, containing 81 000 DPD beads. However, for the explicitly observing toward the inner structure of vesicle aggregates, a larger box of  $34 \times 34 \times 34$  was chosen additionally. The friction coefficient  $\gamma$  and the noise amplitude  $\sigma$  are respectively set to be 4.5 and 3.0, and thus the temperature constant  $k_B T = 1.0$ . The repulsive parameters for the conservative force between DPD

Table 1. Interaction Parameters  $a_{ij}$  (in DPD Units) Used in the Simulations

	A	B	C	S
A	25			
B	50–120	25		
C	80	85–45	25	
S	25	60–400	60	25

particles are defined so as to reproduce segregation between the solvophilic part (A block and solvent) and solvophobic part (B and C blocks). They are listed in Table 1. In this work,  $4 \times 10^5$  DPD steps were carried out so that the computing time is long enough for the system to achieve an equilibrium state.

### 3. RESULTS AND DISCUSSION

In the simulations, the concentration of ABC triblock copolymers was set as 10.0 vol % and kept constant. In order to observe the structural transformations from concentric micelles to bumped micelles, as experiments reported,<sup>35</sup> the DPD simulations reported below were carried out for two cases. One is that the length of B blocks is varied, while the interaction parameters are fixed. The other scenario is that the interaction parameters between B blocks and solvents are changed, while the length of B blocks keeps unchanged. The interaction parameters between different species are shown in Table 1. Without specification, the interaction parameters  $a_{AB}$ ,  $a_{AC}$ , and  $a_{BC}$  were respectively set to be 50.0, 80.0, and 85.0 in the simulations.

**3.1. Effect of Block Length on Morphological Evolution.** In this subsection, the morphological evolutions of the multicompartiment micelles as a function of B block length were investigated. In the simulations, the mutually incompatible B and C blocks are solvophobic, and the interaction parameters  $a_{BS}$  and  $a_{CS}$  are set as 60.0. The solubility of B and C blocks was chosen to be identical, so that the B and C blocks have the same preference for solvents from the viewpoint of interaction enthalpy.

Figure 2 shows the micelle structures observed at different lengths of B blocks. The A, B, and C particles are denoted with green, red, and blue colors, while the solvent particles are omitted. We focused on the results of triblock copolymers with three representative types:  $A_{10}B_yC_z$ ,  $A_5B_yC_z$ , and  $A_2B_yC_z$ . In the figures, the length of solvophobic chains was fixed, i.e.,  $y + z = 10$ . As can be seen from Figure 2a, the ABC triblock copolymers form the concentric structure when B block is longer. Regarding the concentric structure, we observed the spherical micelles (Figure 2a1), cylindrical micelles (Figure 2a2), and vesicles (Figure 2a3), as the A block length decreases from 10 to 5 and to 2. Under this circumstance, B blocks can enwrap all C blocks, resulting in the formation of the structure-in-structure morphologies. As for the smooth vesicles from  $A_2B_6C_4$  polymers, we observed a standard five-layered ABCBA lamellar structure without defects, as clearly shown in the cross section. Figure 2b shows the results for ABC triblock copolymers with shorter B blocks. We observed the raspberry-like spheres (Figure 2b1), raspberry-like cylinders (Figure 2b2), and raspberry-like vesicles (Figure 2b3) at the A block length of 10, 5, and 2, respectively. The raspberry-like structures are denoted as B-bump-C. The C blocks are located inside the micelle core, while B blocks are separated on the C surface to form the bumps. For the raspberry-like vesicles, the

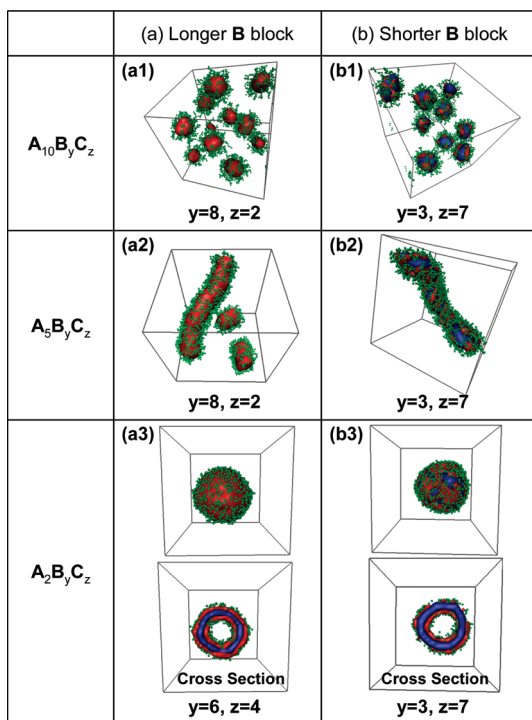


**Figure 2.** Simulated morphologies self-assembled from ABC triblock copolymers with (a) longer and (b) shorter B block length in selective solvents. The interaction parameters are  $a_{BS} = a_{CS} = 60.0$ . The cross sections for the vesicles are also shown. The green, red, and blue colors are respectively assigned to A, B, and C blocks, while the solvents are omitted for clarity.

outside surface is defective with dispersive B bumps, but the inside surface is still smooth (see the cross section of Figure 2b3).

It is apparent from Figure 2 that the self-assembled morphologies of ABC triblock copolymers in selective solvents can change from spherical micelles to cylindrical micelles and to vesicles as the A block length decreases. For each kind of aggregate, we can also observe the structural evolution from concentric to raspberry-like aggregates through decreasing B block lengths. The formation of the raspberry-like structure at shorter B block lengths is due to the fact that B blocks cannot enwrap the C cores sufficiently. If the structures still remain concentric at shorter B block lengths, the B chains would be more stretched in order to cover the C surface completely. This could give rise to an increase in free energy. To alleviate the stretching of B blocks, the B blocks are contracted into bumps on C cores. Therefore, it can be concluded that the evolution from concentric to B-bump-C aggregates is an entropy-dominated process.

In the simulations of the morphological evolutions with decreasing B block lengths, we observed a particular kind of aggregates. That is a novel vesicle from  $A_2B_7C_3$  copolymers, in which B and C blocks are interpenetrative. The detailed structural information is provided in Figure 3. As can be seen from Figure 3a, the outside surface of the vesicle is similarly smooth. The special point can be seen clearly from the cross section. The layer structure is defective, in which the middle C layer is penetrated by B blocks. When only C blocks are shown, a spherical surface with several pores is presented. We defined such vesicle as the inner-penetrating vesicle. In order to obtain detailed information about the microstructure, the density

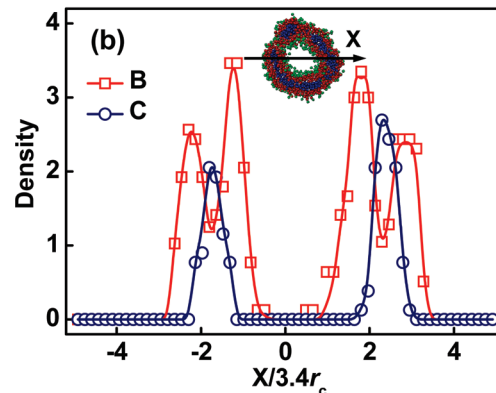
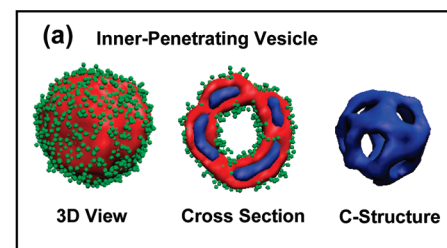


**Figure 3.** (a) Morphology of an inner-penetrating vesicle self-assembled from  $A_2B_7C_3$  triblock copolymer at  $a_{BS} = a_{CS} = 60.0$ . A cross section of the vesicle and the substructure of C blocks are also shown. (b) One-dimensional density profiles along x-arrow of B and C blocks in the inner-penetrating vesicle.

distributions of solvophobic B and C blocks are analyzed. The density profiles are shown in Figure 3b. The inset shows the two-dimensional section of the vesicle, and the coordinate origin denotes the center of vesicle. The profile of B density ( $\varphi_B$ ) displays a tetramodal feature, while C density ( $\varphi_C$ ) displays a bimodal feature. This is typical character of the vesicles. At the maximum points of  $\varphi_C$ , B blocks also have a rich distribution, confirming the interpenetration of B and C blocks. The asymmetrical distribution of C blocks suggests that the penetration is ruleless. Such vesicles were found under the condition that the B blocks are long enough relative to C blocks. The formation can be explained by referring to the raspberry-like micelles. Inside the vesicle, the C blocks cannot maintain a complete layer due to shorter block lengths, and thus they are separated into several pieces to lower the stretching energy.

For the inner-penetrating vesicle, an important application could be drug delivery and release. These pores on C wall can serve as channels for diffuse of B-compatible drugs. If the B blocks can achieve controllable degradation, B-incompatible drugs can also release regularly through these channels. This function may find important applications in controlled release of drugs. Moreover, we found that the structure of the inner-penetrating vesicle is variable. It can be responsive for external stimulations, such as changes in pH and temperature. In the simulations, these changes in pH and temperature can be realized by variations in repulsive interactions between different blocks. The controllable transformation of the vesicle under different conditions is shown explicitly in Figure 4. We chose the inner-penetrating vesicle as an initial state (Figure 4b). When the  $a_{BC}$  decreases from 85 to 45 (which may correspond to decrease of temperature or increase in pH), the vesicular morphology evolves from the inner-penetrating to prolate-smooth with

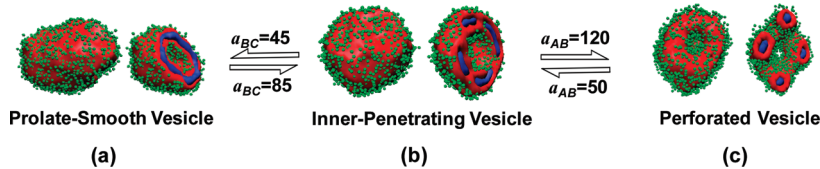


**Figure 4.** Transformation of the multicompartiment vesicles through changing the conditions: (a)  $a_{BC} = 45.0$ ,  $a_{AB} = 50.0$  (prolate-smooth vesicle); (b)  $a_{BC} = 85.0$ ,  $a_{AB} = 50.0$  (inner-penetrating vesicle); (c)  $a_{BC} = 85.0$ ,  $a_{AB} = 120.0$  (perforated vesicle).

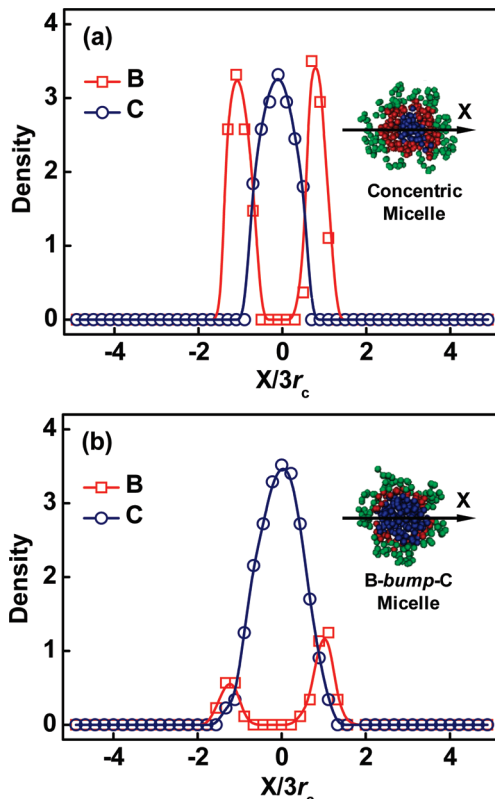


**Figure 5.** One-dimensional density profiles along x-arrows of B and C blocks for the (a) concentric micelle self-assembled from  $A_{10}B_8C_2$  triblock copolymers and the (b) B-bump-C micelle self-assembled from  $A_{10}B_3C_7$  triblock copolymers in selective solvents. The interaction parameters are  $a_{BS} = a_{CS} = 60.0$ .

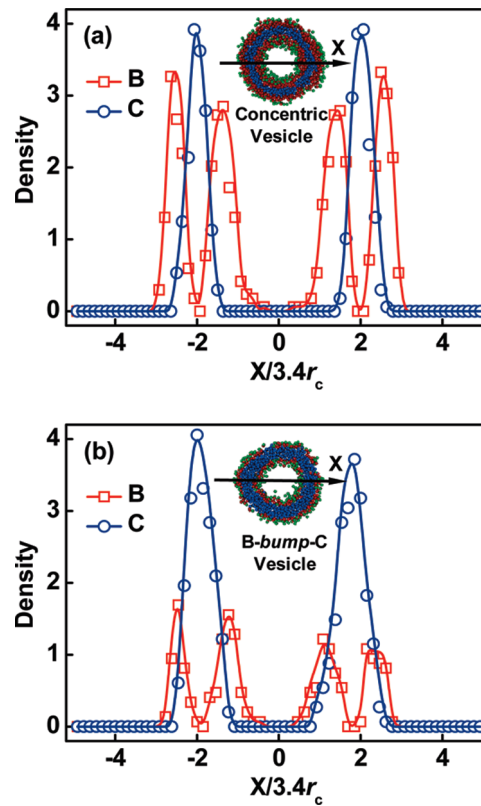


**Figure 6.** One-dimensional density profiles along x-arrows of B and C blocks for the (a) concentric five-layered ABCBA vesicle self-assembled from  $A_2B_6C_4$  triblock copolymers and the (b) raspberry-like vesicle self-assembled from  $A_2B_3C_7$  triblock copolymers in selective solvents. The interaction parameters are  $a_{BS} = a_{CS} = 60.0$ .

C-block pores closed (Figure 4a). Inversely, when the  $a_{BC}$  increases to 85 again, the inner-penetrating vesicle state is resumed. On the other hand, when the  $a_{AB}$  increases from 50 to 120, corresponding to the case like increasing temperature or decreasing pH, the vesicle becomes perforated with pores forming on the entire solvophobic wall (Figure 4c). These pores filled with solvophilic blocks and solvents can be closed by resuming the  $a_{AB}$  interaction. In the two reversible processes, the opening–closing of solvophobic and solvophilic channels are controlled effectively by external stimulations. The vesicles behave like a “*living vesicle*”. They can react vigilantly when facing the varied milieu. Reversible on–off control on the channels of vesicles may make a significant effect on drug loading and releasing in fields of biomaterials.

To get more deep insight into the structural evolution, we analyzed the block density variation in the concentric and B-bump-C spheres. The typical results of the B block density

$\varphi_B$  and C block density  $\varphi_C$  for two types of spherical micelles are shown in Figure 5. When  $a_{BS} = a_{CS} = 60.0$ , the aggregate morphology of  $A_{10}B_8C_2$  copolymers is the concentric sphere. The density distributions of  $\varphi_B$  and  $\varphi_C$  for the sphere structure are illustrated in Figure 5a. The basic building unit of the concentric sphere is a B–C–B layer. The peaks of  $\varphi_B$  almost have the same height with the peak of  $\varphi_C$ . The spherical micelle is chosen arbitrarily at the density calculations, so the density profiles can only give the local microscopic information. Concerning the B-bump-C sphere, the profile of  $\varphi_B$  displays a bimodal feature, while  $\varphi_C$  shows a single peak (see Figure 5b). However, the two peaks of  $\varphi_B$  are much lower than the peak of  $\varphi_C$ , resulting from the formation of raspberry-like structure. The density profiles of B and C blocks for two types of vesicles are presented in Figure 6. Figure 6a shows the typical results for concentric vesicles formed by  $A_2B_6C_4$  triblock copolymers. Density profiles of  $\varphi_B$  and  $\varphi_C$  are symmetric with respect to

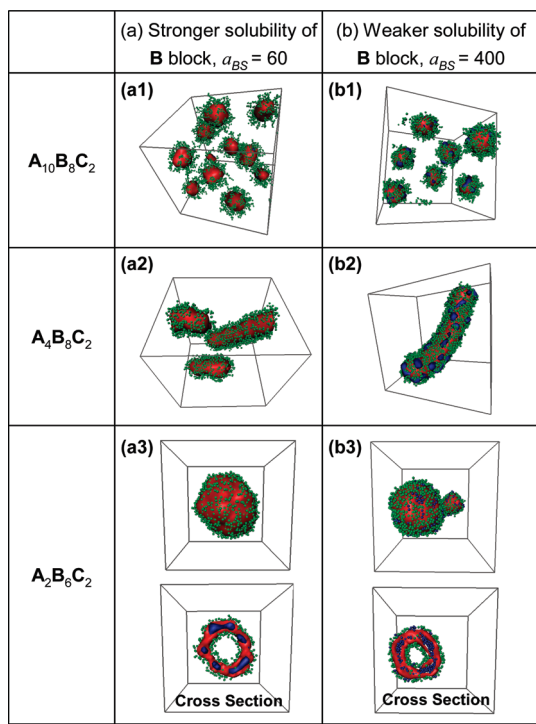


**Figure 7.** Simulated morphologies self-assembled from ABC triblock copolymers with (a)  $a_{BS} = 60.0$  and (b)  $a_{BS} = 400.0$  in selective solvents. The other parameter is  $a_{CS} = 60.0$ .

the center of vesicles. For the raspberry-like vesicles from  $A_2B_3C_7$  triblock copolymers, the peaks of  $\varphi_B$  are much lower than  $\varphi_C$ , as shown in Figure 6b. A slight asymmetry of the density profiles can be observed. This is because of the formation of B-bump-C structure.

Some experimental observations of B-bump-C type aggregates are available in the literature, which are in agreement with our simulation results. Pascault et al. have investigated the raspberry-like micelles formed by a triblock copolymer of polystyrene-*b*-polybutadiene-*b*-poly(methyl methacrylate) (PS-*b*-PB-*b*-PMMA).<sup>32,33</sup> In the experiments, self-assembly takes place when the copolymer is in a selective solvent of epoxy precursors. In the formed structure, the PS spheres are surrounded by PB nodules, while the PMMA blocks are soluble in the epoxy precursors, forming a swollen shell. When diamine was introduced, the epoxy–amine reaction took place. The epoxy network formed within the shell. The “spheres on spheres” structure thus was formed. Schacher et al. also designed a linear triblock copolymer of polybutadiene-*b*-poly(2-vinylpyridine)-*b*-poly(*tert*-butyl methacrylate) (PB-*b*-P2VP-*b*-PT), where the middle P2VP blocks are shorter than the PB end blocks.<sup>34</sup> In the acetone solution, the raspberry-like micelles with three to six P2VP spheres on PB core were observed. It was explained that the strong incompatibility between PB and P2VP blocks results in the compartmentalization of the P2VP phase. Our simulation results are in good agreement with these experimental observations. Furthermore, we predicted the formation of B-bump-C cylindrical micelles and vesicles. Such kinds of aggregates have not been observed yet, and the predictions may provide guidances for further studies.

### 3.2. Effect of Block Solubility on Morphological Evolution.

In this subsection, the effects of B block solubility on the

morphologies of multicompartment micelles self-assembled from linear ABC triblock copolymers were investigated. The block solubility can be expressed as the interaction strength between polymeric blocks and solvents. In the simulations, the interaction parameters  $a_{CS}$  is fixed as 60.0, while  $a_{BS}$  is set to be either 60.0 or 400.0. At higher  $a_{BS}$  value, i.e.,  $a_{BS} = 400.0$ , the contact between B blocks and solvents becomes less energetically favorable relative to that between C blocks and solvents, in terms of interaction enthalpy.

Figure 7 shows the simulation results of ABC triblock copolymer aggregates at lower and higher values of  $a_{BS}$ . For a given volume fraction of each block, varying  $a_{BS}$  value leads to different morphologies. Three types of molecule models were examined, including  $A_{10}B_8C_2$ ,  $A_4B_8C_2$ , and  $A_2B_6C_2$ . When  $a_{BS}$  value is 60.0, the solubility of B blocks is comparative to that of C blocks. In this sense, the concentric spheres (Figure 7a1), concentric cylinders (Figure 7a2), and inner-penetrating vesicles (Figure 7a3) were observed. As  $a_{BS}$  value increases to 400.0, the self-assembled morphologies are changed. As shown in Figure 7b, the raspberry-like micelles were found. The raspberry-like micelles include the raspberry-like spheres (Figure 7b1), raspberry-like cylinders (Figure 7b2), and raspberry-like vesicles (Figure 7b3). The raspberry-like structure is denoted as C-bump-B, i.e., with C bumps on B surface. The raspberry-like micelles are different from those shown in Figure 2b. Rather than forming B bumps on C surface (Figure 2b), in C-bump-B the C blocks come out from the micelle core and aggregate into C bumps on B surface. Notably, only smaller fraction of C blocks resides near the core/shell interface, and the rest C blocks are located within the core especially in bigger micelles. From the cross section of the vesicle, we can also find this point explicitly.

From Figure 7, we know that the increase in  $a_{BS}$  value can lead to an evolution from the concentric micelles (or inner-penetrating vesicles) to raspberry-like micelles (or raspberry-like vesicles). The formation mechanism of these raspberry-like C-bump-B aggregates is different from those of the foregoing B-bump-C one. The formation of C-bump-B aggregates at higher  $a_{BS}$  is enthalpy favorable. At higher value of  $a_{BS}$ , the solubility of C blocks is much better than that of B blocks. Thus, the C blocks tend to be located at solvophobic/solvophilic interface, resulting in the formation of C-bump-B structures. The formation of C-bump-B structures would effectively reduce the unfavorable interaction between the more solvophobic B blocks and solvents, as compared with the concentric structures. However, the accommodation of C blocks on B surface could lead to a higher entropic loss of ABC triblock copolymers, and thus portion of C blocks still remains in the micelle cores. This is the reason why we found the C blocks not only reside on the B surface but also reside inside the micelle cores at higher  $a_{BS}$  value. Therefore, the evolution from concentric to C-bump-B aggregates is an enthalpy-dominated process.

For the sake of understanding the aggregates in detail and demonstrating the inner structure diversity, the density profiles of solvophobic B and C blocks for two typical spherical micelles and two typical vesicles were plotted in Figures 8 and 9. When  $a_{BS} = 60.0$ ,  $A_{10}B_8C_2$  triblock copolymers self-assemble into the concentric spherical micelles. The density profiles of  $\varphi_B$  and  $\varphi_C$  are shown in Figure 8a. Bimodal and unimodal features are shown for the curves of  $\varphi_B$  and  $\varphi_C$ , respectively. The curves are almost symmetric with respect to the center of micelles. Figure 8b shows the density profiles of the C-bump-B sphere at  $a_{BS} = 400.0$ . A bimodal curve of  $\varphi_B$  and a trimodal curve of  $\varphi_C$  can be seen. The specific point is that the density profile of  $\varphi_C$

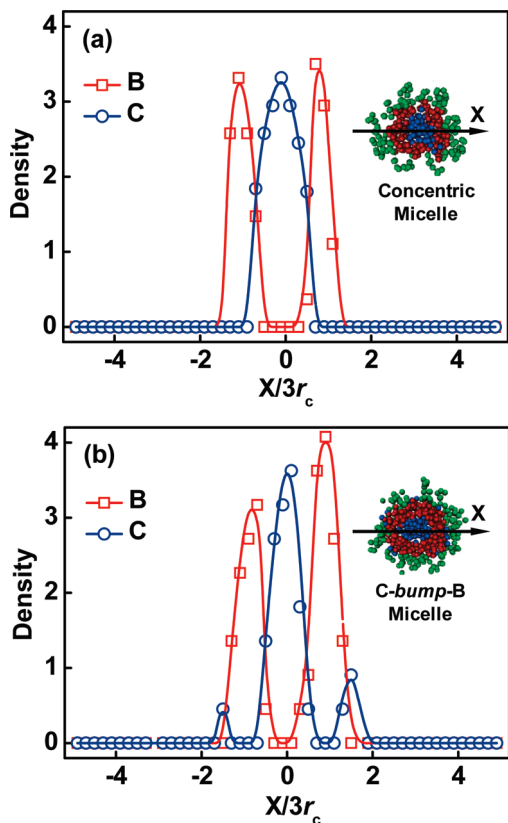


**Figure 8.** One-dimensional density profiles along  $x$ -arrows of B and C blocks for the (a) concentric micelle ( $a_{BS} = a_{CS} = 60.0$ ) and the (b) C-bump-B micelle ( $a_{BS} = 400.0$  and  $a_{CS} = 60.0$ ) self-assembled from  $A_1B_8C_2$  triblock copolymers in selective solvents.

possesses three peaks: one higher peak inside the micelle core and two lower peaks outside the micelle shell. It is proved quantitatively that only a few C domains distribute at the core/shell interface, while the rest C blocks are concentrated in the center of the core.

The density distributions for two typical vesicles at different interaction parameters are given in Figure 9. Figures 9a and 9b show density profiles of formed inner-penetrating and raspberry-like vesicles from  $A_2B_6C_2$  triblock copolymers at  $a_{BS} = 60.0$  and 400.0, respectively. It is known that the inner-penetrating vesicles can form when the length of B blocks is much longer than C blocks. In the C-bump-B structure, the B blocks are the matrix, and C blocks disperse on the surface. In order to express the structure-on-structure explicitly, we chose longer B blocks but shorter C blocks, i.e.,  $A_2B_6C_2$ . For this block copolymer, we calculated the evolution from inner-penetrating to C-bump-B vesicle. As can be seen from Figure 9a, at the maximum points of  $\varphi_C$ , the densities of B blocks are still high, which is the typical character of inner-penetrating vesicle. Figure 9b shows the results of C-bump-B vesicles. The density profiles of  $\varphi_C$  displays a tetramodal rather than bimodal feature, with two higher peaks in the middle layer of vesicle and two lower peaks at the interface of solvophilic leaf/solvophobic wall. This indicates that within the C-bump-B vesicle the C blocks mainly distribute in the wall center, while only a few come out. The C-bump-B spheres show the same character (Figure 8b).

Recently, Laschewsky et al. reported an experimental observation of the C-bump-B structures.<sup>30</sup> The raspberry-like structure

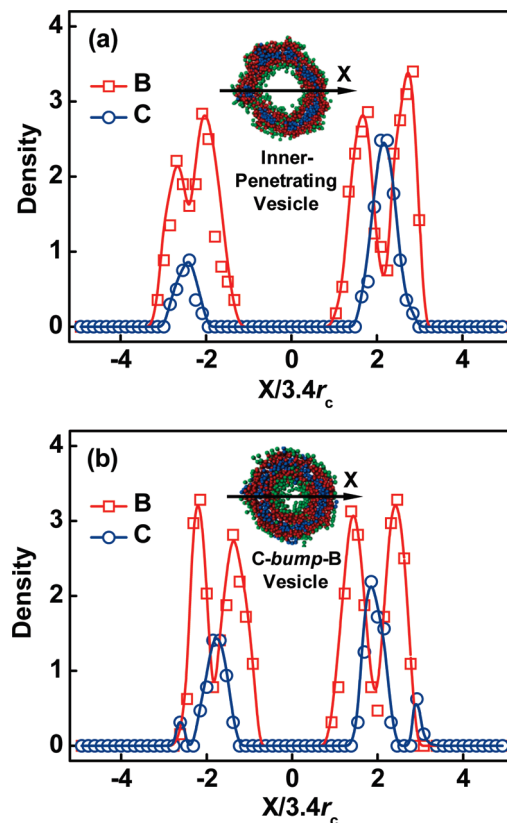


**Figure 9.** One-dimensional density profiles along  $x$ -arrows of B and C blocks for the (a) inner-penetrating vesicle ( $a_{BS} = a_{CS} = 60.0$ ) and the (b) raspberry-like vesicles ( $a_{BS} = 400.0$  and  $a_{CS} = 60.0$ ) self-assembled from  $A_2B_6C_2$  triblock copolymers in selective solvents.

was self-assembled from a linear triblock copolymer consisting of a long cationic solvophilic poly(4-methyl-4-(4-vinylbenzyl)morpholin-4-ium chloride) (PVBM) and two short consecutive solvophobic blocks: a hydrocarbon polystyrene (PS) and a mixed hydrocarbon/fluorocarbon poly(pentafluorophenyl 4-vinylbenzyl ether) (PVBFP). In the micelle core, many small fluorocarbon-rich spheres are located on the surface of the large hydrocarbon-rich sphere. The structure results from the strong segregation between hydrocarbon and fluorocarbon components. On the basis of the cryo-TEM images, it is concluded that the small spheres comprise only the fluorocarbon moieties of PVBFP with the diameter standard of micelles. Each large sphere contains both the hydrocarbon moieties of PS and PVBFP. In addition, Ma et al. obtained the raspberry-like spheres with polystyrene domains dispersed on the polybutadiene surface in the polystyrene-*b*-polybutadiene-*b*-poly(2-vinylpyridine) (PS-*b*-PB-*b*-P2VP) solution.<sup>38</sup> Mixtures of toluene and methanol with the same volume proportion were chosen as the selective solvent, good for P2VP but poor for PS and PB. The weaker solubility of PB than PS favors the formation of raspberry-like multicompartiment micelles. The general character of the two experimental observations is that one solvophobic blocks segregate at the surface of another solvophobic blocks in a bumpy manner and also has rich distribution inside the core. We well reproduced the general features of the raspberry-like structures. That is the fact that in the C-bump-B micelles fewer C blocks reside near the core/shell interface, while the rest C blocks locate within the core. Furthermore, we revealed the microscopic distribution of

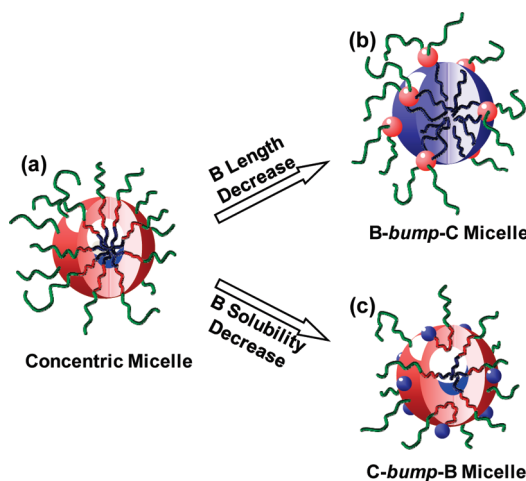


**Figure 10.** Sketch of morphological evolutions of multicompartiment micelles.

blocks by density profiles and the aggregate formation mechanism. We hope the mechanism could be validated in the future experimental studies.

The structural evolution of multicompartiment micelles self-assembled from the triblock copolymers in selective solvents can be illustrated explicitly by the schematic diagram shown in Figure 10. When ABC triblock copolymers are in a selective solvent for A blocks, the concentric micelles with core–shell–corona structure can be formed. As B block length decreases, the aggregates transform from concentric micelles (Figure 10a) to raspberry-like B-bump-C micelles (Figure 10b). On the other hand, as the solubility of B blocks decreases, the raspberry-like C-bump-B micelles were observed (Figure 10c). Raspberry-like micelles are a kind of multicompartiment micelles. Attaining the complex microstructures through ordinary design can effectively satisfy the practical demands. In this work, we predicted various raspberry-like structures from triblock copolymer solutions. The morphological window of triblock copolymers is expanded further. The systematic research on the formation mechanism of raspberry-like micelles contributes to the elucidation of the exact inner structure. In addition, the simulation results provide useful guidances for developing promising strategies to control the raspberry-like structures, which may find potential applications in biomaterials and nanotechnologies. For example, the obtained responsive vesicle (“*living vesicle*”) can be a promising candidate as drug carrier with more sophisticated and smarter controllable release behaviors in applications of the drug delivery systems.

#### 4. CONCLUSIONS

We employed the dissipative particle dynamics method to investigate the morphological transformation from concentric to raspberry-like multicompartiment micelles of linear ABC triblock copolymers in selective solvents. Both the effects of the length and the solubility of B blocks on the aggregate structures were studied. For the first case, the concentric micelles are formed at longer B block length, while the structures with B blocks distributed separately upon C surface (B-bump-C) appears at shorter B block length. In the evolution with increasing B block length, an inner-penetrating vesicle was discovered at relatively shorter C block length. The formation of raspberry-like

structures is entropy-dominated. For the second case, as the  $a_{BS}$  values are much higher than the  $a_{CS}$  values, the C blocks tend to emerge upon B surface and therefore form a C-bump-B structure. It was found that only a smaller fraction of C domains reside near the core/shell interface, and the rest are located within the center of the core. The formation of C-bump-B structures is enthalpy favorable. Our results reveal the mechanism behind the formation of raspberry-like micelles and may provide useful information for preparation of the complex multicompartiment micelles.

#### ■ AUTHOR INFORMATION

##### Corresponding Author

\*Tel +86-21-64253370; Fax +86-21-64251644; e-mail jlin@ecust.edu.cn, jplinlab@online.sh.cn.

#### ■ ACKNOWLEDGMENT

This work was supported by National Natural Science Foundation of China (50925308). Support from the Projects of Shanghai Municipality (09XD1401400, 0952 nm05100, B502, and 08DZ2230500) is also appreciated.

#### ■ REFERENCES

- (1) Kong, W.; Li, B.; Jin, Q.; Ding, D.; Shi, A.-C. *Langmuir* **2010**, *26*, 4226–4232.
- (2) Lorenzo, A. T.; Müller, A. J.; Priftis, D.; Pitsikalis, M.; Hadjichristidis, N. *J. Polym. Sci., Part A: Polym. Chem.* **2007**, *45*, 5387–5397.
- (3) Park, J. Y.; Liu, M.; Mays, J.; Dadmun, M.; Advincula, R. *Soft Matter* **2009**, *5*, 747–749.
- (4) Blanazs, A.; Armes, S. P.; Ryan, A. J. *Macromol. Rapid Commun.* **2009**, *30*, 267–277.
- (5) Pispas, S.; Sarantopoulou, E. *Langmuir* **2007**, *23*, 7484–7490.
- (6) Zhao, F.; Xie, D.; Zhang, G.; Pispas, S. *J. Phys. Chem. B* **2008**, *112*, 6358–6362.
- (7) Wang, J.; Guo, K.; An, L.; Müller, M.; Wang, Z.-G. *Macromolecules* **2010**, *43*, 2037–2041.
- (8) Discher, D. E.; Eisenberg, A. *Science* **2002**, *297*, 967–973.
- (9) LaRue, I.; Adam, M.; Zhulina, E. B.; Rubinstein, M.; Pitsikalis, M.; Hadjichristidis, N.; Ivanov, D. A.; Gearba, R. I.; Anokhin, D. V.; Sheiko, S. S. *Macromolecules* **2008**, *41*, 6555–6563.
- (10) Ding, W.; Lin, S.; Lin, J.; Zhang, L. *J. Phys. Chem. B* **2008**, *112*, 776–783.
- (11) Müller, F.; Delsanti, M.; Auvray, L.; Yang, J.; Chen, Y. J.; Mays, J. W.; Deme, B.; Tirrell, M.; Guenoun, P. *Eur. Phys. J. E* **2000**, *3*, 45–53.
- (12) Wang, L.; Lin, J. *Soft Matter* **2011**, *7*, 3383–3391.
- (13) Kong, W.; Li, B.; Jin, Q.; Ding, D.; Shi, A.-C. *J. Am. Chem. Soc.* **2009**, *131*, 8503–8512.
- (14) Laschewsky, A. *Curr. Opin. Colloid Interface Sci.* **2003**, *8*, 274–281.
- (15) Lutz, J.-F.; Laschewsky, A. *Macromol. Chem. Phys.* **2005**, *206*, 813–817.
- (16) Li, Z.; Kesselman, E.; Talmon, Y.; Hillmyer, M. A.; Lodge, T. P. *Science* **2004**, *306*, 98–101.
- (17) Saito, N.; Liu, C.; Lodge, T. P.; Hillmyer, M. A. *ACS Nano* **2010**, *4*, 1907–1912.
- (18) Cai, Y.; Armes, S. P. *Macromolecules* **2004**, *37*, 7116–7122.
- (19) Sfika, V.; Tsitsilianis, C. *Macromolecules* **2004**, *37*, 9551–9560.
- (20) Breiner, U.; Krappe, U.; Jakob, T.; Abetz, V.; Stadler, R. *Polym. Bull.* **1998**, *40*, 219–226.
- (21) Patrickios, C. S.; Hertler, W. R.; Abbott, N. L.; Hatton, T. A. *Macromolecules* **1994**, *27*, 930–937.
- (22) Kriz, J.; Masar, B.; Plestil, J.; Tuzar, Z.; Pospisil, H.; Doskocilova, D. *Macromolecules* **1998**, *31*, 41–51.

- (23) Yu, G.; Eisenberg, A. *Macromolecules* **1998**, *31*, 5546–5549.
- (24) Gohy, J.-F.; Willet, N.; Varshney, S.; Zhang, J.-X.; Jérôme, R. *Angew. Chem., Int. Ed.* **2001**, *40*, 3214–3216.
- (25) Liu, S.; Armes, S. P. *J. Am. Chem. Soc.* **2001**, *123*, 9910–9911.
- (26) Gohy, J.-F.; Lohmeijer, B. G. G.; Varshney, S. K.; Décamps, B.; Leroy, E.; Boileau, S.; Schubert, U. S. *Macromolecules* **2002**, *35*, 9748–9755.
- (27) Zhou, Z.; Li, Z.; Ren, Y.; Hillmyer, M. A.; Lodge, T. P. *J. Am. Chem. Soc.* **2003**, *125*, 10182–10183.
- (28) Lodge, T. P.; Hillmyer, M. A.; Zhou, Z. *Macromolecules* **2004**, *37*, 6680–6682.
- (29) Skrabania, K.; v. Berlepsch, H.; Böttcher, C.; Laschewsky, A. *Macromolecules* **2010**, *43*, 271–281.
- (30) Kubowicz, S.; Baussard, J.-F.; Thünemann, A. F.; v. Berlepsch, H.; Lutz, J.-F.; Laschewsky, A. *Angew. Chem., Int. Ed.* **2005**, *44*, 5262–5265.
- (31) v. Berlepsch, H.; Böttcher, C.; Skrabania, K.; Laschewsky, A. *Chem. Commun.* **2009**, 2290–2292.
- (32) Ritzenthaler, S.; Court, F.; David, L.; Girard-Reydet, E.; Leibler, L.; Pascault, J. P. *Macromolecules* **2002**, *35*, 6245–6254.
- (33) Ritzenthaler, S.; Court, F.; Girard-Reydet, E.; Leibler, L.; Pascault, J. P. *Macromolecules* **2003**, *36*, 118–126.
- (34) Schacher, F.; Walther, A.; Ruppel, M.; Drechsler, M.; Müller, A. H. E. *Macromolecules* **2009**, *42*, 3540–3548.
- (35) Schacher, F.; Walther, A.; Müller, A. H. E. *Langmuir* **2009**, *25*, 10962–10969.
- (36) Schacher, F.; Betthausen, E.; Walther, A.; Schmalz, H.; Pergushov, D. V.; Müller, A. H. E. *ACS Nano* **2009**, *3*, 2095–2102.
- (37) Uchman, M.; Stepanek, M.; Prochazka, K. *Macromolecules* **2009**, *42*, 5605–5613.
- (38) Ma, Z.; Yu, H.; Jiang, W. *J. Phys. Chem. B* **2009**, *113*, 3333–3338.
- (39) Gohy, J.-F.; Khousakoun, E.; Willet, N.; Varshney, S. K.; Jérôme, R. *Macromol. Rapid Commun.* **2004**, *25*, 1536–1539.
- (40) Skrabania, K.; Laschewsky, A.; v. Berlepsch, H.; Böttcher, C. *Langmuir* **2009**, *25*, 7594–7601.
- (41) Lin, S.; Numasawa, N.; Nose, T.; Lin, J. *Macromolecules* **2007**, *40*, 1684–1692.
- (42) Wang, L.; Lin, J.; Zhang, L. *Langmuir* **2009**, *25*, 4735–4742.
- (43) Zhang, L.; Lin, J.; Lin, S. *Macromolecules* **2007**, *40*, 5582–5592.
- (44) Cui, J.; Jiang, W. *Langmuir* **2010**, *26*, 13672–13676.
- (45) Yin, Y.; Jiang, R.; Li, B.; Jin, Q.; Ding, D.; Shi, A.-C. *J. Chem. Phys.* **2008**, *129*, 154903.
- (46) Wang, R.; Tang, P.; Qiu, F.; Yang, Y. *J. Phys. Chem. B* **2005**, *109*, 17120–17127.
- (47) Ma, Z.; Jiang, W. *J. Polym. Sci., Part B: Polym. Phys.* **2009**, *47*, 484–492.
- (48) Chou, S.-H.; Tsao, H.-K.; Sheng, Y.-J. *J. Chem. Phys.* **2006**, *125*, 194903.
- (49) Li, X.; Pivkin, I. V.; Liang, H.; Karniadakis, G. E. *Macromolecules* **2009**, *42*, 3195–3200.
- (50) Xin, J.; Liu, D.; Zhong, C. *J. Phys. Chem. B* **2007**, *111*, 13675–13682.
- (51) Li, X.; Liu, Y.; Wang, L.; Deng, M.; Liang, H. *Phys. Chem. Chem. Phys.* **2009**, *11*, 4051–4059.
- (52) Zhao, Y.; Liu, Y.-T.; Lu, Z.-Y.; Sun, C.-C. *Polymer* **2008**, *49*, 4899–4909.
- (53) Hoogerbrugge, P. J.; Koelman, J. M. V. A. *Europhys. Lett.* **1992**, *19*, 155–160.
- (54) Koelman, J. M. V. A.; Hoogerbrugge, P. J. *Europhys. Lett.* **1993**, *21*, 363–368.
- (55) Sheng, Y. J.; Nung, C. H.; Tsao, H. K. *J. Phys. Chem. B* **2006**, *110*, 21643–21650.
- (56) Groot, R. D.; Warren, P. B. *J. Chem. Phys.* **1997**, *107*, 4423–4435.
- (57) Allen, M. P.; Tildesley, D. J. *Computer Simulation of Liquids*; Clarendon Press: Oxford, 1987.
- (58) Español, P.; Warren, P. *Europhys. Lett.* **1995**, *30*, 191–196.